

Overcoming limitations in propane dehydrogenation by co-designing catalysts/membrane systems

Authors: Rawan Almallahi^{1,2}, James Wortman^{1,2}, Suljo Linic^{1,2,*}.

Affiliations:

¹ Department of Chemical Engineering, University of Michigan, Ann Arbor, Michigan, United States.

² Catalysis Science and Technology Institute, University of Michigan, Ann Arbor, Michigan, United States.

* Correspondence to: linic@umich.edu.

Abstract: Propylene production through propane dehydrogenation (PDH) is endothermic, and high temperatures required to achieve acceptable propane conversions lead to low selectivity and severe carbon-induced deactivation of conventional catalysts. We developed a catalyst/membrane system that removes the hydrogen by-product and can thus achieve propane conversions that exceed equilibrium limitations. In this codesigned system, a $\text{SiO}_2/\text{Al}_2\text{O}_3$ hollow-fiber hydrogen membrane was packed with a selective $\text{Pt}_1\text{Sn}_1/\text{SiO}_2$ PDH catalyst on the tube side with hydrogen diffusing from the tube to the shell side. We demonstrate that the catalyst/membrane system can achieve propane conversions $>140\%$ of the nominal equilibrium conversion with a propylene selectivity $>98\%$ without deactivation of the membrane. We also show that by introducing oxygen on the shell side of the membrane/catalyst system, we can couple the endothermic PDH reaction on the tube side with the exothermic hydrogen oxidation on the shell side. This coupling results in higher rates of hydrogen transport leading to further enhancements in the propane conversion as well as desired thermoneutral system operation.

One-Sentence Summary: We report a catalyst/membrane system that can overcome thermodynamic limitations imposed on propane dehydrogenation with enhanced stability and selectivity and potential for thermoneutral operation.

Main Text:

Propylene, used in the production of polypropylene, propylene oxide, and acrylonitrile (1), has been produced from petroleum through large-scale centralized steam and fluid catalytic cracking (2). However, the recent surge in shale gas has caused a shift in feedstock from naphtha to shale-based ethane. Steam cracking of ethane results in little to no propylene production, leading to the so-called propylene supply gap where the demand for propylene is projected to be higher than the supply (3).

One way to alleviate this problem is to develop technologies that can convert propane, another shale gas component, directly into propylene in a distributed fashion that is commensurate with the shale gas supply chain (4, 5). A technology that meets these objectives is catalytic propane dehydrogenation (PDH), where propane is directly converted to propylene and hydrogen (H₂). PDH is an endothermic reaction requiring elevated reaction temperatures to achieve acceptable propane conversions (**Fig. S1**). Under these high temperature conditions, the rates of undesired side reactions, such as propane cracking and the formation of solid carbon on the catalyst surface, are more thermodynamically favored (**Fig. S2**), leading to low selectivity and rapid catalyst deactivation, requiring frequent and costly catalyst regeneration (6–9). For example, the commercial Catofin chromium-based catalytic process alternates between dehydrogenation, regeneration, and purge steps within 15- to 30-min cycles (10). Various catalyst active site design strategies to increase activity and stability have recently been shown, and we refer to several review papers in this area for a more detailed summary (1–2, 11).

Beyond the active site, coupling catalysis with separation functionality (for example, a permselective membrane) is a promising strategy for achieving outcomes that may not be achievable in traditional fixed- or fluidized-bed reactors. (12–14). In the case of PDH, a strategy that specifically addresses the problem of low equilibrium conversion is to couple a PDH catalyst to a H₂-permeable membrane to form a catalyst/membrane chemical conversion system (15, 16). In this design, H₂ molecules, formed during PDH, are removed from the reaction zone with a separation membrane that shifts the reaction equilibrium toward the product side and enhances propane conversion. This approach also reduces downstream separation requirements (separating propane and propylene is challenging) and costs. The membrane/catalyst system can also be operated at higher propane feed pressures, which is generally avoided because higher pressure leads to lower equilibrium conversions, so less catalyst and smaller reactor volumes can be used. Finally, lower operating temperatures may be possible, which would limit undesired high temperature cracking and catalyst poisoning side reactions (17).

Despite these advantages, there are numerous obstacles to implementing this catalyst/membrane strategy. One obstacle is the limited availability of selective H₂ transporting membranes that can operate under these conditions. Previous studies have attempted to employ metal-based (palladium) (16, 18–20), zeolite (20–22), and oxide-based membranes (16, 18, 23, 24) with very limited success due to high cost, chemical reactivity that results in low product selectivity and susceptibility to deactivation by carbon deposition (coking) under PDH conditions (15, 18). In addition, commercial PDH catalysts are not viable for these systems because they are designed to operate with extra H₂ added to the reactant stream. For example, platinum (Pt)-based PDH catalysts (used in the Oleflex process) require additional H₂ to alleviate some of the problems with catalyst stability (25, 26). This addition of H₂ is unsuitable for catalyst/membrane systems which require a catalyst that can operate in a H₂ depleted regime (27).

We recently reported the development of a selective PDH catalyst that operates at the thermodynamic conversion limit with the propylene selectivity of >99% without any addition of H₂ (28). The catalyst consisted of small (~ 2 nm diameter) Pt₁Sn₁ nanoparticles (NPs) supported on silica (SiO₂) (28). In this work, we demonstrate the design of a multifunctional catalyst/membrane system that can operate at conversions that exceed the nominal thermodynamic limits of PDH at a given temperature. The catalyst/membrane system consists of the Pt₁Sn₁/SiO₂ PDH catalyst co-designed with a catalyst-compatible SiO₂-based H₂ permeable hollow fiber membrane. We show that the membrane selectively removes H₂ produced during the PDH reaction on the catalyst, at meaningful removal rates, and shifts the PDH equilibrium towards a higher propane conversion and propylene yields.

We also discuss how the development of these membrane/catalysts systems allows us to expand the operational PDH temperature range to lower temperatures and incorporate exothermic oxidation of removed H₂, while retaining high conversion and reaction rates. This lower temperature operation improved the stability of the materials under the harsher, reducing catalyst/membrane system reaction conditions. Incorporating H₂ oxidation allows us to couple the endothermic PDH reaction on the tube side with the exothermic hydrogen oxidation on the shell side. This coupling results in higher rates of hydrogen transport leading to further enhancements in the propane conversion as well as desired thermoneutral system operation. Finally, we shed light on several issues related to the development of efficient catalyst/membrane systems, demonstrating the need for the co-design and co-optimization of the catalytic and transport functionalities.

Catalyst/membrane design

An effective catalyst/membrane system relies on codesigning catalytic and separation functionalities to achieve optimal performance. A practical system should have high volumetric PDH reaction rates and high H₂ removal rates, so the membrane needs to have a high surface area for transporting H₂ without compromising catalyst surface area. This goal can be accomplished by using hollow fiber membranes with small diameters packed with a PDH catalyst inside the hollow fiber membrane. These hollow fiber geometries allow for high membrane surface areas per volume of reactor (>1000 m²/m³) which can decrease overall reactor volumes to achieve desired conversions (21, 29).

The catalyst/membrane hollow fiber system (**Fig. 1A**) consists of an asymmetric and porous Al₂O₃ tubular hollow fiber with a thin SiO₂ separation layer on the inner side of the tube. The SiO₂ layer selectively separates H₂ from propane and propylene. The PDH catalyst was packed inside the fiber on the SiO₂ membrane side. The Al₂O₃ tube consisted of two Al₂O₃ layers (dimensions shown in **Fig. S3**): an outer layer of ~860 µm with a 200 nm average pore size distribution, and an inner ~10 µm layer with a 20 nm average pore size distribution. The SEM image of the inner surface in the Al₂O₃ tube shows a clear porous surface (**Fig. 1B**), whereas the SEM image of the outer surface shows large particles with a large pore size distribution (**Fig. 1C**). We deposited SiO₂ on the inner side of the Al₂O₃ tube through chemical vapor deposition (CVD) of tetraethyl orthosilicate (TEOS) at 600 °C (**Fig. S4-6**). A thin (~ 500 nm) SiO₂ separation layer formed on the inner side of the Al₂O₃ tube (**Fig. 1D**).

We established that the deposited SiO_2 covered the entire inner surface of the porous Al_2O_3 tube. The SEM image of the inner surface of the $\text{SiO}_2/\text{Al}_2\text{O}_3$ membrane (**Fig. 1E**) shows a smooth layer with a very small pore size distribution and no pinholes or cracks. The complete covering of the Al_2O_3 inner side with the SiO_2 separation layer was also confirmed using x-ray photoelectron spectroscopy. The XPS spectra associated with the characteristic Si 2p (**Fig. 1F**) and Al 2p peaks (**Fig. 1G**) for the SiO_2 -coated and uncoated Al_2O_3 tubes, respectively, showed that no Al peaks were detected for the SiO_2 -coated sample (also see **Fig. S7 and S8**). The x-ray diffraction (XRD) pattern of the $\text{SiO}_2/\text{Al}_2\text{O}_3$ membrane in **Fig. S9** only showed the spectra for the Al_2O_3 substrate because the topmost SiO_2 layer was amorphous.

The PDH catalyst was composed of SiO_2 -supported Pt_1Sn_1 NPs described previously (28). Approximately 250 mg of the $\text{Pt}_1\text{Sn}_1/\text{SiO}_2$ PDH catalyst was packed inside the hollow fiber membrane on the tube side (where propane is fed), along the entire length of the tube. On the other side of the tube (shell side), an inert Ar sweep gas was used to carry the separated H_2 . The $\text{SiO}_2/\text{Al}_2\text{O}_3$ membrane allows for some diffusion (backflow) of Ar to the inner tube side, so we needed to account for this backflow-induced dilution of the reactive mixture in the calculations of the equilibrium propane conversion.

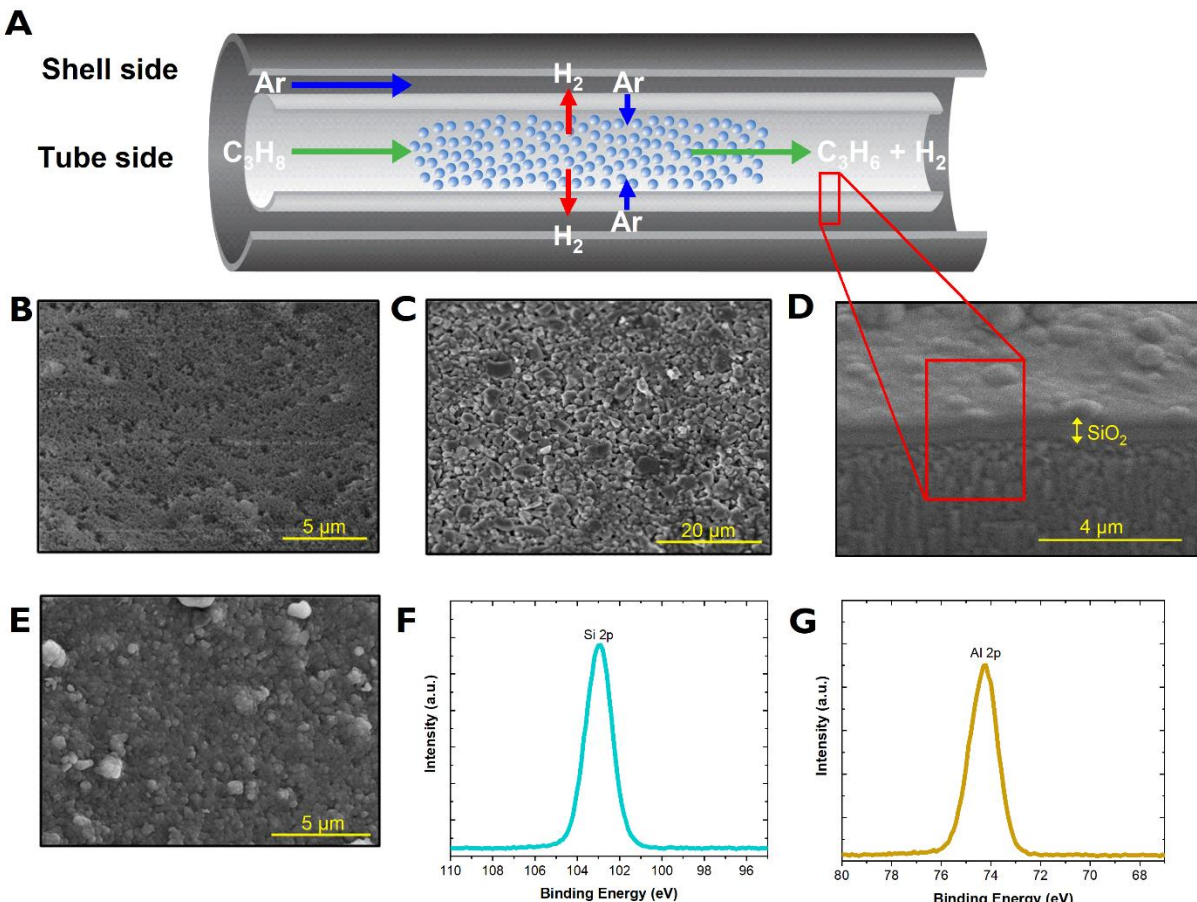


Fig. 1. Catalyst/membrane system and $\text{SiO}_2/\text{Al}_2\text{O}_3$ hollow fiber membrane characterization. (A) Coupled catalyst/membrane system schematic. (B) Inner surface SEM image of the uncoated Al_2O_3 hollow fiber membrane (before SiO_2 deposition). (C) Outer surface, (D) cross-section and

(E) inner surface SEM images of the $\text{SiO}_2/\text{Al}_2\text{O}_3$ hollow fiber membrane showing the porous alumina substrate, layered $\text{SiO}_2/\text{Al}_2\text{O}_3$ structure, and the topmost smooth SiO_2 layer, respectively. **(F)** Si 2p photoemission spectra of $\text{SiO}_2/\text{Al}_2\text{O}_3$ hollow-fiber membrane. **(G)** Al 2p photoemission spectra of the uncoated Al_2O_3 hollow fiber membrane.

Membrane performance

Data in **Fig. 2** show the performance of the SiO_2 based membrane in separating $\text{H}_2/\text{C}_3\text{H}_8$ mixtures. Data in **Fig. 2A** show H_2 permeability and $\text{H}_2/\text{C}_3\text{H}_8$ separation factors measured at a total flow rate of $10 \text{ cm}^3/\text{min}$ of an equimolar mixture of $\text{H}_2/\text{C}_3\text{H}_8$ at a sweep:feed ratio of 6. The sweep rate is the rate at which the inert sweep gas is moved on the shell side, removing gases that permeate through the membrane. At 580°C where PDH is often operated, the $\text{SiO}_2/\text{Al}_2\text{O}_3$ hollow fiber membrane exhibited a H_2 permeability of $\sim 2 \cdot 10^{-7} \text{ mol/m}^2 \text{ s Pa}$ and a $\text{H}_2/\text{C}_3\text{H}_8$ separation factor of 19.

The data in **Fig. 2B** show the membrane performance was stable during the study (~ 20 hours). To put these separation factors in context, we compare them in **Fig. 2C** (and **Fig. 2A**) to the Knudsen separation limit, which represents the maximum separation that can be achieved by using the Knudsen effect. Our results show the $\text{SiO}_2/\text{Al}_2\text{O}_3$ hollow fiber membranes exceeded these limits substantially. We attribute these high separation factors to two effects. First, the higher sweep-induced flow rate change created a driving force that drove H_2 through the membrane that was greater than the driving force to diffuse propane, so the partial pressure of H_2 (P_{H_2}) was lowered on the shell side. Second, molecular sieving occurred because the pores in the silica membrane were small enough to effectively exclude C_3 molecules and selectively diffuse only H_2 . We refer to **Fig. S10** for details on deposition procedures for the membranes, and Eq. S1-S3 for definitions of membrane performance metrics. For the hollow fiber dimensions used herein, 60 minutes was chosen as the optimal deposition period for selective separation. Shorter deposition times were insufficient to fully coat silica on the fibers, while longer deposition times would introduce mass transfer limitations.

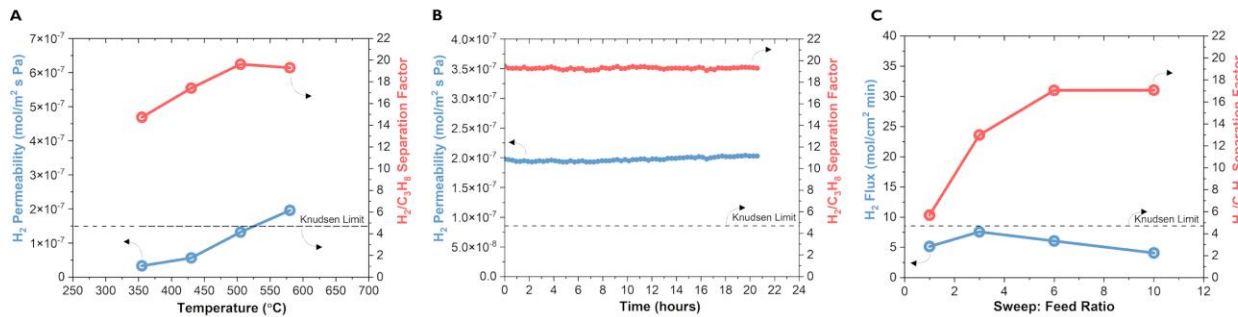


Fig. 2. $\text{SiO}_2/\text{Al}_2\text{O}_3$ hollow fiber membrane characterization. **(A)** H_2 permeability and the $\text{H}_2/\text{C}_3\text{H}_8$ separation factor as a function of temperature and **(B)** time for an equimolar mixture of H_2 and C_3H_8 ($5 \text{ cm}^3/\text{min}$ each) and an Ar sweep on the shell side ($60 \text{ cm}^3/\text{min}$) and **(C)** sweep: feed ratios (Ar sweep varied between 10 to $100 \text{ cm}^3/\text{min}$ on the shell side) at $T = 580^\circ\text{C}$. (Note that error bars are standard deviation of multiple gas chromatography runs on the same membrane.)

Catalytic performance

Data in **Fig. 3A** show the performance of the catalyst/membrane system in PDH at 580 °C, measured at pure propane feed (slightly diluted by Ar backflow discussed above), sweep:feed ratios between 4 to 10 and a constant weight hourly space velocity (WHSV) of 1.3 h⁻¹. WHSV is defined as the mass of propane entering the reactor per unit time divided by the mass of the catalyst in the reactor. The different sweep:feed ratios were obtained by varying the Ar sweep gas flow rate on the shell side between 12 to 50 cm³/min. We also show that the nominal thermodynamic limit on propane conversion under these reaction conditions (dashed black line) ranges between 50 to 52%, depending on the amount of Ar diluent present at the different sweep:feed ratios. The data show that at these conditions, the catalyst/membrane system reached propane conversions of ~ 10% higher (above 60 %) than the equilibrium conversion with >95% propylene selectivity.

Another parameter that can be tuned to improve the H₂ removal rate is the WHSV, because at higher gas residence times (as the WHSV is lowered), a membrane can remove higher fractions of H₂ produced during the reaction. Data in **Fig. 3B** show the performance of the catalyst/membrane system for PDH at 580°C, pure propane feed (diluted by small amounts of Ar backflow), a constant sweep:feed ratio of 10, and with WHSVs changing from 0.86 to 2.16 h⁻¹. The different WHSVs were obtained by varying the propane flow rate on the tube side between 2 and 5 cm³/min for a constant catalyst loading of 250 mg. The data show that as WHSV decreased, propane conversion was substantially increased without sacrificing product selectivity.

Co-optimization studies

These multifunctional catalyst/membrane systems require co-optimization of multiple functionalities. In this case, the catalytic and the H₂ separation functions need to be codesigned, which requires concurrent tuning of multiple system parameters and creates a large design phase space that is difficult to explore. In these situations, it is useful to perform a dimensionless analysis to identify the minimal number of dimensionless variables that can guide the catalyst/membrane design. For catalyst/membrane systems, two dimensionless numbers, the Damkohler (Da) and Peclet (Pe) numbers, are sufficient to capture the design space (31–34). The Da number is described by the ratio of the reaction rate and the convective transport rate of the reactant through the reactor. It is closely related to the conversion that can be achieved in a system, with a larger Da number leading to larger conversion. The Pe number is the ratio of convective transport rate to the membrane permeation rate. A combination of high Da and low Pe numbers are desired for optimized performance, marked by a high reaction rate and a high H₂ permeation rate.

Data in **Fig. 3C** show the measured propylene yield in the catalyst/membrane system as a function Da and Pe dimensionless numbers (calculated using Eqs. S7 and S8). Those data were obtained at 580°C, with a pure propane stream (diluted by small amounts of Ar backflow). The Da and Pe numbers were varied by changing the WHSVs between 0.86 and 2.16 h⁻¹ and sweep:feed ratios between 4 to 10. By changing the sweep:feed ratio, we changed the H₂ partial pressure difference across the membrane, which affected the Pe number, whereas changing WHSV impacted both the Da and Pe numbers.

The data in Fig. 3C show that an improved performance is seen at higher Da and lower Pe (29, 31) and that at 580°C the highest propylene yield of 65% was achieved, which is 10% above the equilibrium limit (assuming 100% selectivity to propylene) of 55%. Therefore, we concluded that for the hollow fiber catalyst/membrane tubular geometries analyzed herein, at 580°C, the

enhancement factors in propylene yield, of $\sim 10\%$ above equilibrium conversion, are realistic. These enhancements could be further improved by making the diameter of the hollow fiber membranes smaller or designing better performing membranes – we note that there are reports of SiO_2 -based membranes achieving 2 to 3 times higher H_2 permeability and separation factors of 500 or higher, which would further lower the Pe number. (35)

To assess the practical utility of this multicomponent catalyst/membrane chemical conversion system, it is critical to compare it in a systematic way to its alternatives. A performance metric that is often used to quantify the performance of a catalyst is the forward rate of propane conversion per gram of the catalyst. We analyzed the inherent kinetic PDH reaction rates, using an integral reactor analysis (28), for many reported catalysts (18–20, 22, 24, 28, 36–63) and compared them to the rates measured on the $\text{Pt}_1\text{Sn}_1/\text{SiO}_2$ catalyst used in the membrane system herein. The data in **Fig. 3D** and **Table S1** show that the PDH rates in our system (pink stars) are comparable to the best performing Pt-based PDH catalysts (blue triangles), and substantially higher than the rates on non-Pt based materials (green and yellow symbols).

Another critical figure of merit in PDH is the selectivity to propylene as a function of propane conversion. Data in **Fig. 3E** and **Table S2** show the initial selectivity/conversion performance resulted for different reported PDH systems. The data show that the catalyst/membrane system analyzed herein outperformed other systems with respect to selectivity/conversion performance metrics. For example, at 580°C , the catalyst/membrane system reached $\sim 123\%$ propane conversion (relative to nominal equilibrium conversion) with $> 95\%$ propylene selectivity. The performance could be even further improved relative to the thermodynamic equilibrium limit to $> 140\%$ conversion with $> 98\%$ propylene selectivity by lowering the temperature to 500°C . As shown in Fig. 3E, this performance exceeds other PBR catalysts and catalyst/membrane systems previously tested for propane dehydrogenation, which in general suffer from poor selectivity or conversion (20, 22–24).

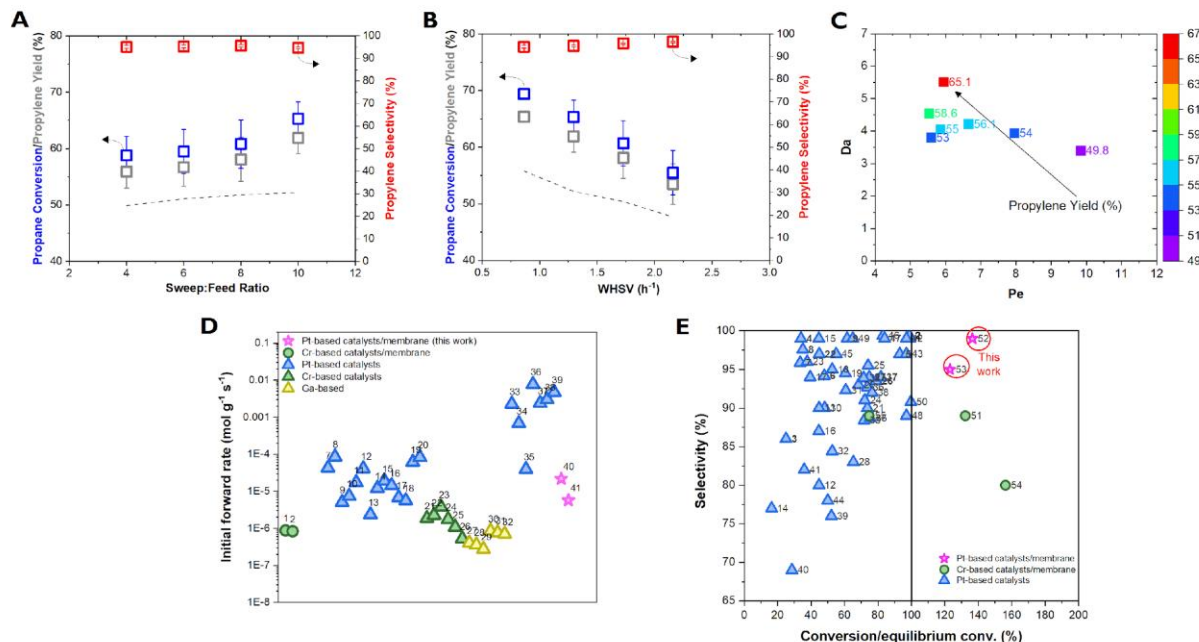


Fig. 3. Catalyst/Membrane hollow fiber system performance in propane dehydrogenation. (A) Propane conversion, propylene selectivity and propylene yield as a function of sweep:feed ratios (WHSV = 1.3 hours⁻¹) compared to reaction equilibrium limit (dashed line) calculated for the same experimental conditions. (B) Propane conversion, propylene selectivity and propylene yield as a function of WHSV (sweep:feed = 10) compared to reaction equilibrium limit (dashed line) calculated for the same experimental conditions. (Note that error bars are standard deviation after replication of three catalyst loadings.) (C) Propylene yield as a function of dimensionless Da and Pe. (D) Initial reaction rate for various membrane/catalyst systems and PBR catalysts reported in the literature. Numbers correspond to row numbers in Table S1. Two data points from this work are for the catalyst/membrane system at 580° and 500°C (points 40 and 41, respectively). (E) Conversion-selectivity plots for different PDH catalysts. Numbers in the figure correspond to row numbers in Table S2.

Stability studies

Another crucial performance metric that has prevented serious commercial considerations for catalyst/membrane systems is their poor stability under carbon-rich, reducing PDH reaction conditions, which lead to formation of solid carbon deposits. These harsh conditions are further exacerbated by the removal of H₂. Previous studies of catalyst/membrane systems addressed these difficulties in several ways, such as substantially diluting the propane feed, reporting the initial time data points only, and often co-feeding H₂, which defeats the purpose of using the catalyst/membrane systems to shift equilibrium conversion (17–20, 23, 24).

Data in **Fig. 4A** show propane conversion, propylene selectivity and yield as a function of time obtained with our Pt₁Sn₁/SiO₂ catalyst/membrane system at 580°C, in a pure propane stream, a WHSV of 1.3 h⁻¹ and a sweep:feed ratio of 10. The catalyst/membrane system deactivated slowly over a time of ~22 hours. In **Table S1**, we compared the rate of deactivation of the catalyst/membrane system discussed herein to the measured rates of deactivation of other systems [analyzed using first-order deactivation kinetics (2)]. The data in Table S1 show that the stability of the Pt₁Sn₁/SiO₂ catalyst/membrane system, although not completely stable, exceeded the other catalyst/membrane systems, even those that resorted to feed dilution and co-feeding H₂ (17–20, 23, 24).

The decline in the performance of the catalyst/membrane system 580°C (Fig. 4A) was likely related to a gradual deactivation of the catalyst as solid carbon formed on its surface, which is a general feature of PDH processes. This hypothesis was supported by data in **Fig. 4B** which show that the performance of the membrane was stable over time under the reaction conditions, that is, the measured H₂ removal rate and the H₂/C₃H₈ separation factor as a function of time were relatively constant. The slight decrease in the H₂ removal rate in Fig. 4B over time was the result of decreasing propane conversion that produced less H₂.

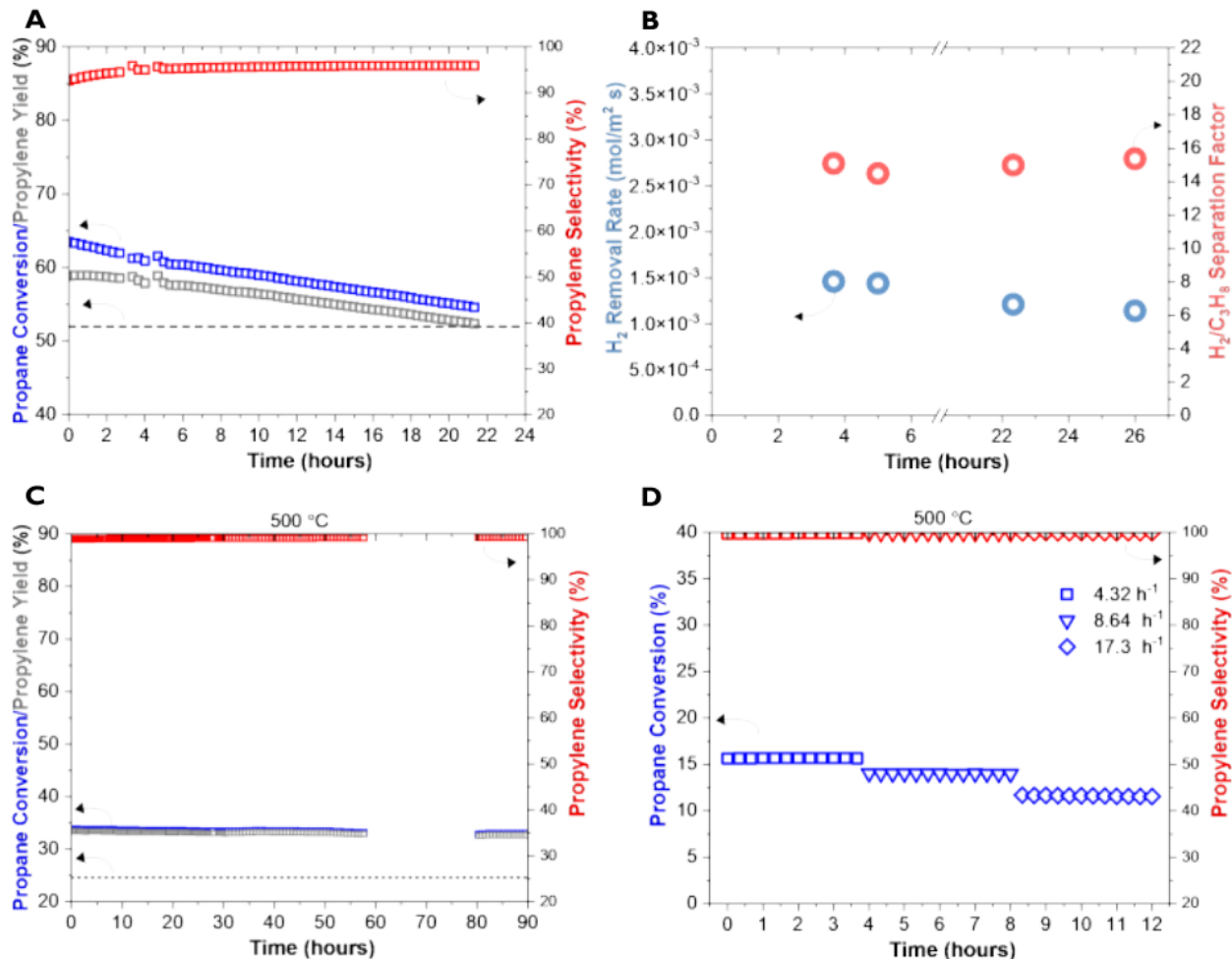


Fig. 4. Stability and low temperature performance of catalyst/membrane hollow fiber system. (A) Propane conversion, propylene selectivity and propylene yield as a function of time for the catalyst/membrane hollow fiber system compared to the equilibrium limit calculated for the same conditions (dashed line). (B) H₂ removal rate and the H₂/C₃H₈ separation factor as a function of time for the catalyst/membrane hollow fiber system. For (A) & (B), reaction temperature = 580°C, P_{C₃H₈} = 1 atm, WHSV = 1.3 hours⁻¹ and sweep: feed = 10. (C) Propane conversion, propylene selectivity and yield as a function of time for the catalyst/membrane hollow fiber system compared to the equilibrium limit calculated for the same conditions (dashed line). The missing data from ~ 58 to 80 hrs were the result of a GC gas tank running out over a weekend. Reaction temperature = 500°C, P_{C₃H₈} = 1 atm, WHSV = 0.43 hours⁻¹ and sweep: feed ratio = 10. (D) Propane conversion and propylene selectivity as a function of time for the catalyst/membrane hollow fiber system at different WHSVs. Reaction temperature = 500°C, P_{C₃H₈} = 1 atm, and sweep flow rate = 100 cm³/min.

Carbon-induced deactivation in dehydrogenation catalysis can be limited by operating at lower temperature (64–67). An added benefit of lower temperature operation is reduced energy input (68–71), but the main drawback is a decline in propane equilibrium conversion. We hypothesized that catalyst/membrane systems are ideal for lower temperature operations, since higher propane conversions can be achieved at a given temperature given that the catalyst/membrane systems can bypass equilibrium limits, as shown above and as simulated in **Fig. S11**.

Data in **Fig. 4C** show propane conversion, propylene selectivity, and yield as a function of time at 500 °C, in a pure propane stream, a WHSV of 0.43 h⁻¹ and a sweep: feed ratio of 10 for the catalyst/membrane system (open blue and red squares). The data show that contrary to performance at 580°C, the system exhibited remarkable stability at these lower temperatures with >99% propylene selectivity. We compared the operation of the catalyst/membrane system to the thermodynamic equilibrium limit at 500°C. The data showed that the catalyst/membrane system operated above the equilibrium limit by ~9 % higher conversion (~141 % relative to equilibrium conversion) without noticeable deactivation for >90 hours on stream. This membrane/catalyst system achieved the same conversion at 500°C that would require 530°C, assuming the equilibrium conversion. The measured conversion levels at these conditions are comparable to commercial PDH processes, which are achieved at higher temperatures, and that suffer from rapid deactivation, even when operating with additional H₂ in the reactant stream (1).

More rigorous testing of catalyst stability requires that the system is antagonized under higher propane flow rate conditions, i.e., at the conditions where the catalyst is processing higher volumes of propane per unit time (away from equilibrium conversion). The data in **Fig. 4D** show that the catalyst/membrane system exhibited stable performance even as the flow rates increased. Expectedly, these increased flow rates led to lower conversions. In simple terms, our measurements show that at 500 °C, the catalyst/membrane system is relatively stable with low deactivation rates at near 100 % selectivity to propylene.

To further demonstrate the flexibility offered by this catalyst/membrane reacting systems designs, we explored coupling the propane dehydrogenation reaction on the tube side with the H₂ oxidation on the shell side by introducing diluted O₂ in the sweeping gas (**Fig. 5A**). The introduction of O₂, which at these temperatures reacts with H₂ to form water provides a twofold opportunity. One advantage is that it creates a larger driving force for the H₂ transport from the tube to the shell side because H₂ is consumed in the reaction with O₂. In addition, the exothermic H₂ oxidation provides heat for the endothermic PDH, i.e., the coupling of the two reactions could allow for a thermoneutral operation. Data in **Figure 5B** show the performance of the catalyst/membrane system measured at 500 °C for a pure propane feed on the tube side, sweep:feed ratio of 12 with 0-10% molar O₂ concentration in the sweep gas and a constant WHSV of 0.86 h⁻¹. We note that the total sweep gas flow rate was maintained at 24 cm³/min for experiments performed with different amounts of O₂.

The data show that in the pure N₂ sweep (no O₂ added), the catalyst/membrane system reached a propane conversion of ~28% (marked by the dashed blue line), which is 6% above the equilibrium conversion, with > 99% propylene selectivity. After O₂ was introduced in the N₂ sweep on the shell side, higher propane conversions were obtained, reaching ~ 34% for 10% O₂. Under these conditions propylene selectivity was very high: about 96.5% based on the carbon balance. We hypothesize these greater propane conversions were the result of increasing H₂ removal from the tube to the shell side because of the consumption of H₂ by O₂ in the oxidation reaction (see **Figure S15** for hydrogen removal rates). To support this hypothesis, we measured the molar ratio of H₂O to CO₂ formed in the reacting systems and found that it was between 3.5 and 4.2, which means that O₂ is mainly reacting with H₂ (i.e., on the shell side) since oxidation of propane or propylene would lead to ratios of 1.33 or 1 respectively. These data are shown in **Figure S15**. We note that the addition of steam during PDH may help alleviate coke formation, although this was not the intent of this study. (2,72)

Using measured water formation rates, material balances and reaction rates, along with tabulated heats of reactions for all endothermic and exothermic reactions taking place in the catalyst/membrane system, we performed an energy balance analysis to establish the conditions required for the thermoneutral operation (calculation details are included in the supplement). Data in **Fig. 5C** show the energy required to sustain PDH and energy released from H₂ oxidation reactions as a function of the amount of O₂ in the sweep. When no O₂ was present (0% O₂), PDH required considerable energy to be sustained at these temperatures (the orange vertical bar). As O₂ is introduced, as PDH conversion increased, the energy required to support the reactions was also increased. The data in the table show that for this specific system and under these conditions (i.e., the measured rates of reactions and selectivity) when the concentration of O₂ in the sweep reached 10 %, the energy released by H₂ oxidation (green bars) became sufficient to drive the endothermic PDH reaction. An important advantage of the hollow fiber design is that moving energy (heat) through these systems should be facile and controllable given the small dimensions of the tubes.

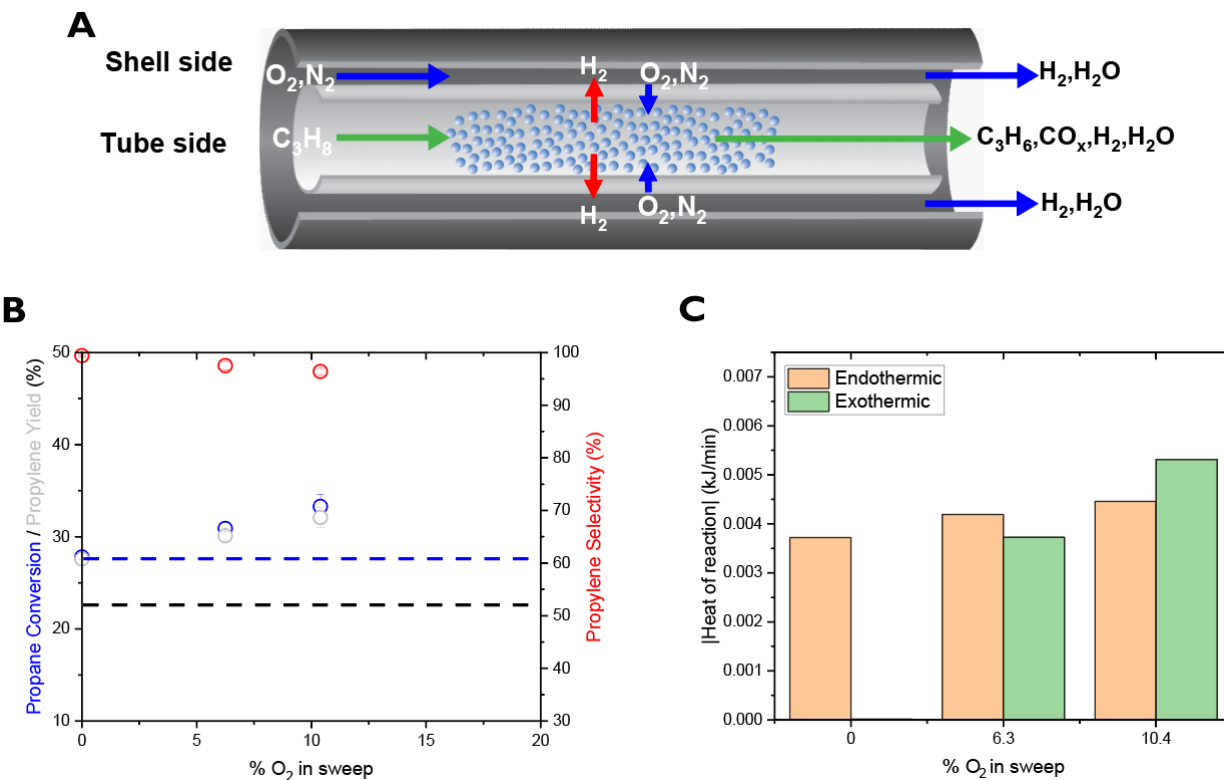


Fig. 5. Catalyst/membrane hollow fiber system performance and heat calculations for propane dehydrogenation and coupled hydrogen combustion. (A) Coupled catalyst/membrane system for PDH and H₂ oxidation schematic. (B) Propane conversion, propylene selectivity and propylene yield as a function of % O₂ introduced in the inert sweep compared to reaction equilibrium limit (dashed black line) and the case with no O₂ (dashed blue line). (C) Heat requirement for propane dehydrogenation and heat release from combustion of H₂ and propane oxidation as a function of % O₂ introduced in the inert sweep. Reaction temperature = 500 °C, P_{C₃H₈} = 1 atm, WHSV = 0.86 hours⁻¹ and sweep:feed ratio = 12.

Discussion

In conclusion, we demonstrate an approach towards codesigning a catalytic and separation functionality for PDH that allows us to move beyond equilibrium conversion limits. We also show that the catalyst/membrane systems permit us to expand temperature range for viable operation, allowing us to decrease system deactivation due to carbon coking, and to incorporate exothermic H₂ oxidation. Rigorous technoeconomic costs and benefit analysis of a membrane/catalyst system will be crucial to understand its practical utility. On one hand, adding a membrane to a PDH catalyst will increase the reactor unit complexity. On the other hand, potential technoeconomic benefits of the membrane/catalyst PDH systems include: (i) the ability to operate at higher pressures (and therefore lower Pt catalyst loadings and smaller reactor volumes) compared to commercial PDH processes, which are operated only at 1-3 atm due to equilibrium limitations; (ii) the ability to seamlessly integrate exothermic hydrogen oxidation on the permeate side, which would increase the H₂ permeation driving force and reduce the need for interstage heating; (iii) similar heat transfer benefits can also be achieved if steam is used as the sweeping fluid; and (iv) the decreased downstream separations cost associated with the demanding propane/propylene and C₃/H₂ separations. These factors, along with the enhancement in stability and viable temperature operating range demonstrated here, offer substantial opportunities for improving yields and energy efficiencies in PDH processes.

References and Notes

1. S. Chen, X. Chang, G. Sun, T. Zhang, Y. Xu, Y. Wang, C. Pei, J. Gong, Propane dehydrogenation: catalyst development, new chemistry, and emerging technologies. *Chem Soc Rev.* **50**, 3315–3354 (2021).
2. J. J. H. B. Sattler, J. Ruiz-Martinez, E. Santillan-Jimenez, B. M. Weckhuysen, Catalytic Dehydrogenation of Light Alkanes on Metals and Metal Oxides. *Chem Rev.* **114**, 10613–10653 (2014).
3. E. National Academies of Sciences and Medicine, *The Changing Landscape of Hydrocarbon Feedstocks for Chemical Production: Implications for Catalysis: Proceedings of a Workshop* (The National Academies Press, Washington, DC, 2016; <https://www.nap.edu/catalog/23555/the-changing-landscape-of-hydrocarbon-feedstocks-for-chemical-production-implications>).
4. Office of Oil and Natural Gas, Office of Fossil Energy, “Natural Gas Flaring and Venting: State and Federal Regulatory Overview, Trends, and Impacts” (2019).
5. R. Mansoor, M. Tahir, Recent Developments in Natural Gas Flaring Reduction and Reformation to Energy-Efficient Fuels: A Review. *Energy & Fuels.* **35**, 3675–3714 (2021).
6. Z.-J. Zhao, C. Chiu, J. Gong, Molecular understandings on the activation of light hydrocarbons over heterogeneous catalysts. *Chem Sci.* **6**, 4403–4425 (2015).
7. F. Jiang, L. Zeng, S. Li, G. Liu, S. Wang, J. Gong, Propane Dehydrogenation over Pt/TiO₂–Al₂O₃ Catalysts. *ACS Catal.* **5**, 438–447 (2014).
8. J. Wang, X. Chang, S. Chen, G. Sun, X. Zhou, E. Vovk, Y. Yang, W. Deng, Z.-J. Zhao, R. Mu, C. Pei, J. Gong, On the Role of Sn Segregation of Pt-Sn Catalysts for Propane Dehydrogenation. *ACS Catal.* **0**, 4401–4410 (2021).
9. A. Iglesias-Juez, A. M. Beale, K. Maaijen, T. C. Weng, P. Glatzel, B. M. Weckhuysen, A combined *in situ* time-resolved UV–Vis, Raman and high-energy resolution X-ray absorption spectroscopy study on the deactivation behavior of Pt and PtSn propane dehydrogenation catalysts under industrial reaction conditions. *J Catal.* **276**, 268–279 (2010).

10. M. M. Bhasin, J. H. McCain, B. v Vora, T. Imai, P. R. Pujadó, Dehydrogenation and oxydehydrogenation of paraffins to olefins. *Appl Catal A Gen.* **221**, 397–419 (2001).
11. Sun, M.-L., Hu, Z.-P., Wang, H.-Y., Suo, Y.-J. & Yuan, Z.-Y. Design Strategies of Stable Catalysts for Propane Dehydrogenation to Propylene. *ACS Catal.* **13**, 4719–4741 (2023).
12. Wortman, J., Igenegbai, V. O., Almallahi, R., Motagamwala, A. H. & Linic, S. Optimizing hierarchical membrane/catalyst systems for oxidative coupling of methane using additive manufacturing. *Nat. Mater.* **22**, 1523–1530 (2023).
13. Igenegbai, V. O., Almallahi, R., Meyer, R. J. & Linic, S. Oxidative Coupling of Methane over Hybrid Membrane/Catalyst Active Centers: Chemical Requirements for Prolonged Lifetime. *ACS Energy Lett.* 1465–1470 (2019)
14. Igenegbai, V. O., Meyer, R. J. & Linic, S. In search of membrane-catalyst materials for oxidative coupling of methane: Performance and phase stability studies of gadolinium-doped barium cerate and the impact of Zr doping. *App. Catal. B: Environ.* **230**, 29–35 (2018).
15. J. N. Armor, Applications of catalytic inorganic membrane reactors to refinery products. *J Memb Sci.* **147**, 217–233 (1998).
16. H. Weyten, J. Luyten, K. Keizer, L. Willems, R. Leysen, Membrane performance: the key issues for dehydrogenation reactions in a catalytic membrane reactor. *Catal Today.* **56**, 3–11 (2000).
17. Z. D. Ziaka, R. G. Minet, T. T. Tsotsis, A high temperature catalytic membrane reactor for propane dehydrogenation. *J Memb Sci.* **77**, 221–232 (1993).
18. J. P. Collins, R. W. Schwartz, R. Sehgal, T. L. Ward, C. J. Brinker, G. P. Hagen, C. A. Udovich, Catalytic Dehydrogenation of Propane in Hydrogen Permselective Membrane Reactors. *Industrial & Engineering Chemistry Research.* **35**, 4398–4405 (1996).
19. E. Gbenedio, Z. Wu, I. Hatim, B. F. K. Kingsbury, K. Li, A multifunctional Pd/alumina hollow fibre membrane reactor for propane dehydrogenation. *Catal Today.* **156**, 93–99 (2010).
20. S. Pati, N. Dewangan, Z. Wang, A. Jangam, S. Kawi, Nanoporous Zeolite-A Sheltered Pd-Hollow Fiber Catalytic Membrane Reactor for Propane Dehydrogenation. *ACS Appl Nano Mater.* **3**, 6675–6683 (2020).
21. Z. Wang, J. Xu, S. Pati, T. Chen, Y. Deng, N. Dewangan, L. Meng, J. Y. S. Lin, S. Kawi, High H₂ permeable SAPO-34 hollow fiber membrane for high temperature propane dehydrogenation application. *AIChE Journal.* **66**, e16278 (2020).
22. S.-J. Kim, Y. Liu, J. S. Moore, R. S. Dixit, J. G. Pendergast, D. Sholl, C. W. Jones, S. Nair, Thin Hydrogen-Selective SAPO-34 Zeolite Membranes for Enhanced Conversion and Selectivity in Propane Dehydrogenation Membrane Reactors. *Chemistry of Materials.* **28**, 4397–4402 (2016).
23. R. Schäfer, M. Noack, P. Kölsch, M. Stöhr, J. Caro, Comparison of different catalysts in the membrane-supported dehydrogenation of propane. *Catal Today.* **82**, 15–23 (2003).
24. H. Weyten, K. Keizer, A. Kinoo, J. Luyten, R. Leysen, Dehydrogenation of propane using a packed-bed catalytic membrane reactor. *AIChE Journal.* **43**, 1819–1827 (1997).
25. C. Li, G. Wang, Dehydrogenation of light alkanes to mono-olefins. *Chem Soc Rev.* **50**, 4359–4381 (2021).
26. Q. Li, Z. Sui, X. Zhou, Y. Zhu, J. Zhou, D. Chen, Coke Formation on Pt–Sn/Al₂O₃ Catalyst in Propane Dehydrogenation: Coke Characterization and Kinetic Study. *Top Catal.* **54**, 888 (2011).
27. A. Sattler, M. Paccagnini, E. Gomez, R. J. Meyer, S. Yacob, H. Klutse, M. Caulfield, Y. Gao, Catalytic limitations on alkane dehydrogenation under H₂ deficient conditions relevant to membrane reactors. *Energy Environ Sci.* **15**, 2120–2129 (2022).

28. A. H. Motagamwala, R. Almallahi, J. Wortman, V. O. Igenegbai, S. Linic, Stable and selective catalysts for propane dehydrogenation operating at thermodynamic limit. *Science* (1979). **373**, 217 (2021).
29. S.-W. Choi, D. S. Sholl, S. Nair, J. S. Moore, Y. Liu, R. S. Dixit, J. G. Pendergast, Modeling and process simulation of hollow fiber membrane reactor systems for propane dehydrogenation. *AICHE Journal*. **63**, 4519–4531 (2017).
30. J. Kärger, D. M. Ruthven, D. N. Theodorou, "Diffusion in Nanoporous Materials" in *Diffusion in Nanoporous Materials* (Wiley-VCH, 2012), vol. 1, pp. 85–110.
31. S. Battersby, P. W. Teixeira, J. Beltramini, M. C. Duke, V. Rudolph, J. C. Diniz da Costa, An analysis of the Peclet and Damkohler numbers for dehydrogenation reactions using molecular sieve silica (MSS) membrane reactors. *Catal Today*. **116**, 12–17 (2006).
32. Y. v Gokhale, R. D. Noble, J. L. Falconer, Effects of reactant loss and membrane selectivity on a dehydrogenation reaction in a membrane-enclosed catalytic reactor. *J Memb Sci*. **103**, 235–242 (1995).
33. W. S. Moon, S. bin Park, Design guide of a membrane for a membrane reactor in terms of permeability and selectivity. *J Memb Sci*. **170**, 43–51 (2000).
34. S.-W. Choi, C. W. Jones, S. Nair, D. S. Sholl, J. S. Moore, Y. Liu, R. S. Dixit, J. G. Pendergast, Material properties and operating configurations of membrane reactors for propane dehydrogenation. *AICHE Journal*. **61**, 922–935 (2015).
35. Vos, R. M. de & Verweij, H. High-Selectivity, High-Flux Silica Membranes for Gas Separation. *Science*. **279**, 1710–1711 (1998).
36. Z. Wu, I. M. D. Hatim, B. F. K. Kingsbury, E. Gbenedio, K. Li, A novel inorganic hollow fiber membrane reactor for catalytic dehydrogenation of propane. *AICHE Journal*. **55**, 2389–2398 (2009).
37. O. A. Bariås, A. Holmen, E. A. Blekkan, Propane Dehydrogenation over Supported Pt and Pt–Sn Catalysts: Catalyst Preparation, Characterization, and Activity Measurements. *J Catal*. **158**, 1–12 (1996).
38. J. Salmones, J.-A. Wang, J. A. Galicia, G. Aguilar-Rios, H₂ reduction behaviors and catalytic performance of bimetallic tin-modified platinum catalysts for propane dehydrogenation. *J Mol Catal A Chem*. **184**, 203–213 (2002).
39. Y. Zhou, S. M. Davis, Low-Pressure Dehydrogenation of Light Paraffins (1993).
40. N. Kaylor, R. J. Davis, Propane dehydrogenation over supported Pt–Sn nanoparticles. *J Catal*. **367**, 181–193 (2018).
41. Y. Zhang, Y. Zhou, L. Huang, M. Xue, S. Zhang, Sn-Modified ZSM-5 As Support for Platinum Catalyst in Propane Dehydrogenation. *Industrial & Engineering Chemistry Research*. **50**, 7896–7902 (2011).
42. P. L. de Cola, R. Gläser, J. Weitkamp, Non-oxidative propane dehydrogenation over Pt–Zn-containing zeolites. *Appl Catal A Gen*. **306**, 85–97 (2006).
43. Y. Duan, Y. Zhou, Y. Zhang, X. Sheng, M. Xue, Effect of Sodium Addition to PtSn/AlSBA-15 on the Catalytic Properties in Propane Dehydrogenation. *Catal Letters*. **141**, 120–127 (2011).
44. G. Siddiqi, P. Sun, V. Galvita, A. T. Bell, Catalyst performance of novel Pt/Mg(Ga)(Al)O catalysts for alkane dehydrogenation. *J Catal*. **274**, 200–206 (2010).
45. P. Sun, G. Siddiqi, W. C. Vining, M. Chi, A. T. Bell, Novel Pt/Mg(In)(Al)O catalysts for ethane and propane dehydrogenation. *J Catal*. **282**, 165–174 (2011).
46. D. Shee, A. Sayari, Light alkane dehydrogenation over mesoporous Cr₂O₃/Al₂O₃ catalysts. *Appl Catal A Gen*. **389**, 155–164 (2010).
47. F. J. Pérez-Reina, E. Rodríguez-Castellón, A. Jiménez-López, Dehydrogenation of Propane over Chromia-Pillared Zirconium Phosphate Catalysts. *Langmuir*. **15**, 8421–8428 (1999).

48. M. Alcántara-Rodríguez, E. Rodríguez-Castellón, A. Jiménez-López, Propane Dehydrogenation on Mixed Ga/Cr Oxide Pillared Zirconium Phosphate Materials. *Langmuir*. **15**, 1115–1120 (1999).
49. X. Zhang, Y. Yue, Z. Gao, Chromium Oxide Supported on Mesoporous SBA-15 as Propane Dehydrogenation and Oxidative Dehydrogenation Catalysts. *Catal Letters*. **83**, 19–25 (2002).
50. K. L. Fjdala, T. D. Tilley, Thermolytic molecular precursor routes to Cr/Si/Al/O and Cr/Si/Zr/O catalysts for the oxidative dehydrogenation and dehydrogenation of propane. *J Catal.* **218**, 123–134 (2003).
51. J. J. H. B. Sattler, I. D. González-Jiménez, A. M. Mens, M. Arias, T. Visser, B. M. Weckhuysen, Operando UV-Vis spectroscopy of a catalytic solid in a pilot-scale reactor: deactivation of a CrO_x/Al₂O₃ propane dehydrogenation catalyst. *Chemical Communications*. **49**, 1518–1520 (2013).
52. M. Saito, S. Watanabe, I. Takahara, M. Inaba, K. Murata, Dehydrogenation of Propane Over a Silica-Supported Gallium Oxide Catalyst. *Catal Letters*. **89**, 213–217 (2003).
53. B. Zheng, W. Hua, Y. Yue, Z. Gao, Dehydrogenation of propane to propene over different polymorphs of gallium oxide. *J Catal.* **232**, 143–151 (2005).
54. P. Michorczyk, J. Ogonowski, Dehydrogenation of propane to propene over gallium oxide in the presence of CO₂. *Appl Catal A Gen.* **251**, 425–433 (2003).
55. B. Xu, B. Zheng, W. Hua, Y. Yue, Z. Gao, Support effect in dehydrogenation of propane in the presence of CO₂ over supported gallium oxide catalysts. *J Catal.* **239**, 470–477 (2006).
56. M. Chen, J. Xu, F.-Z. Su, Y.-M. Liu, Y. Cao, H.-Y. He, K.-N. Fan, Dehydrogenation of propane over spinel-type gallia–alumina solid solution catalysts. *J Catal.* **256**, 293–300 (2008).
57. L. Shi, G. Deng, W. Li, S. Miao, Q. Wang, W. Zhang, A. Lu, Al 2 O 3 Nanosheets Rich in Pentacoordinate Al 3+ Ions Stabilize Pt-Sn Clusters for Propane Dehydrogenation. *Angewandte Chemie*. **127**, 14200–14204 (2015).
58. E. J. Jang, J. Lee, H. Y. Jeong, J. H. Kwak, Controlling the acid-base properties of alumina for stable PtSn-based propane dehydrogenation catalysts. *Appl Catal A Gen.* **572**, 1–8 (2019).
59. H. Xiong, S. Lin, J. Goetze, P. Pletcher, H. Guo, L. Kovarik, K. Artyushkova, B. M. Weckhuysen, A. K. Datye, Thermally Stable and Regenerable Platinum–Tin Clusters for Propane Dehydrogenation Prepared by Atom Trapping on Ceria. *Angewandte Chemie International Edition*. **56**, 8986–8991 (2017).
60. L. Liu, M. Lopez-Haro, C. W. Lopes, S. Rojas-Buzo, P. Concepcion, R. Manzorro, L. Simonelli, A. Sattler, P. Serna, J. J. Calvino, A. Corma, Structural modulation and direct measurement of subnanometric bimetallic PtSn clusters confined in zeolites. *Nat Catal.* **3**, 628–638 (2020).
61. L. Deng, H. Miura, T. Shishido, S. Hosokawa, K. Teramura, T. Tanaka, Dehydrogenation of Propane over Silica-Supported Platinum–Tin Catalysts Prepared by Direct Reduction: Effects of Tin/Platinum Ratio and Reduction Temperature. *ChemCatChem*. **6**, 2680–2691 (2014).
62. L. Deng, T. Shishido, K. Teramura, T. Tanaka, Effect of reduction method on the activity of Pt–Sn/SiO₂ for dehydrogenation of propane. *Catal Today*. **232**, 33–39 (2014).
63. L. Liu, M. Lopez-Haro, C. W. Lopes, C. Li, P. Concepcion, L. Simonelli, J. J. Calvino, A. Corma, Regioselective generation and reactivity control of subnanometric platinum clusters in zeolites for high-temperature catalysis. *Nat Mater.* **18**, 866–873 (2019).
64. M. Larsson, M. Hultén, E. A. Blekkan, B. Andersson, The Effect of Reaction Conditions and Time on Stream on the Coke Formed during Propane Dehydrogenation. *J Catal.* **164**, 44–53 (1996).
65. M. P. Lobera, C. Téllez, J. Herguido, M. Menéndez, Transient kinetic modelling of propane dehydrogenation over a Pt–Sn–K/Al₂O₃ catalyst. *Appl Catal A Gen.* **349**, 156–164 (2008).

66. H. P. Rebo, E. A. Blekkan, L. Bednářová, A. Holmen, "Deactivation of Pt-Sn catalyst in propane dehydrogenation" in *Studies in Surface Science and Catalysis*, B. Delmon, G. F. Froment, Eds. (Elsevier, 1999; <https://www.sciencedirect.com/science/article/pii/S0167299199804832>), vol. 126, pp. 333–340.

67. M. van Sint Annaland, J. A. M. Kuipers, W. P. M. van Swaaij, A kinetic rate expression for the time-dependent coke formation rate during propane dehydrogenation over a platinum alumina monolithic catalyst. *Catal Today*. **66**, 427–436 (2001).

68. P. Wang, J. Yao, Q. Jiang, X. Gao, D. Lin, H. Yang, L. Wu, Y. Tang, L. Tan, Stabilizing the isolated Pt sites on PtGa/Al₂O₃ catalyst via silica coating layers for propane dehydrogenation at low temperature. *Appl Catal B*. **300**, 120731 (2022).

69. Z. Song, Q. Wang, C. Guo, S. Li, W. Yan, W. Jiao, L. Qiu, X. Yan, R. Li, Improved Effect of Fe on the Stable NiFe/Al₂O₃ Catalyst in Low-Temperature Dry Reforming of Methane. *Industrial & Engineering Chemistry Research*. **59**, 17250–17258 (2020).

70. H. R. T, G. Georgios, R. Romain, S. Julia, F. Jordan, W. Yicheng, M. Angelos, D. Prashant, C. Phillip, F.-S. Maria, S. Michail, S. E. C. H, First-principles design of a single-atom–alloy propane dehydrogenation catalyst. *Science* (1979). **372**, 1444–1447 (2021).

71. Y. Qu, G. Li, T. Zhao, Z. Zhang, M. Douthwaite, J. Zhang, Z. Hao, Low-Temperature Direct Dehydrogenation of Propane over Binary Oxide Catalysts: Insights into Geometric Effects and Active Sites. *ACS Sustainable Chemistry & Engineering*. **9**, 12755–12765 (2021).

72. Festa, G., Contaldo, P., Martino, M., Meloni, E. & Palma, V. *Ind. Eng. Chem. Res.* **62**, 16622–16637 (2023).

Acknowledgments: Funding: This material is based upon work supported by the US DOE Office of Basic Energy Sciences, Division of Chemical Sciences (DE-SC0021008). The initial work on the project was support by RAPID under Award Number DE-EE0007888. R.A. acknowledges support from the National Science Foundation Graduate Research Fellowship under Grant No. DGE 1256260. The authors acknowledge the technical support from the Michigan Center for Materials Characterization. **Author contributions:** S.L. and R.A. conceived the project and designed the experiments. R.A. and J.W. designed and constructed the reactor used to obtain reaction data. R.A. performed propane dehydrogenation experiments and membrane characterization. All authors analyzed the reaction data and membrane characterization data. S.L. R.A. and J.W. wrote the paper. All authors edited the manuscript. **Competing interests:** A provisional patent application has been filed for this work (U.S. Provisional Application Patent No. 63/378,234). The authors declare no competing interests. **Data and materials availability:** All other data needed to evaluate the conclusions in the paper are present in the paper or the Supplementary Materials.

The Supplementary Materials file includes:

Materials and Methods
 Figs. S1 to S15
 Tables S1 to S2